EFFECTS OF AN ADIABATIC FIN ON THE MIXED CONVECTION HEAT TRANSFER IN A SQUARE CAVITY WITH TWO VENTILATION PORTS

by

Fatih SELIMEFENDIGIL[a]* and Hakan F. OZTOP[b]

[a] Department of Mechanical Engineering, Faculty of Engineering, Celal Bayar University, Manisa, Turkey
[b] Department of Mechanical Engineering, Technology Faculty, Firat University, Elazig, Turkey

Original scientific paper
DOI: 10.2298/TSCI120608047S

In this study, a square cavity with two ventilation ports in the presence of an adiabatic fin of different lengths placed on the walls of the cavity is numerically analyzed for the mixed convection case for a range of Richardson numbers (Ri = 0.1, 1, 10, 100) and at Reynolds number of 300. The effect of the fin height, placement of the fin on each of the four walls of the cavity and Richardson number on the heat transfer and fluid flow characteristics is numerically analyzed. The results are presented in terms of streamlines, isotherm plots, and averaged Nusselt number plots. It is observed that for the convection dominated case, fin length and its position on the one of the four walls of the cavity do not alter the thermal performance whereas when the buoyancy effects become important thermal performance increases for high fin length.

Key words: *mixed convection, adiabatic fin, thermal performance*

Introduction

Mixed convection heat transfer is important for various engineering applications. Design of the heat exchangers, nuclear reactors, solar collectors, cooling of electronic equipments, and food industry may be considered as some of them where one has to improve the thermal performance of those systems.

A vast amount of literature is dedicated to study the heat transfer and flow field characteristics for the mixed convection case and numerical modeling in real case studies [1-8]. Saeidi and Khodadadi [3] have studied the unsteady laminar flow with an square enclosure with two ventilation ports. They showed that for Strouhal number of 0.1, the mean Nusselt numbers on the four walls exhibit large amplitudes of oscillation, but at Strouhal number of 10, the amplitudes of oscillation on various walls are generally degraded. They also showed that, heat transfer enhancement is observed for the range of considered Strouhal numbers. Sourtiji *et al.* [9] have investigated the flow field and heat transfer characteristics in a square cavity with two ventilation ports for the mixed convection case. A pulsating velocity is imposed at the inlet port for

* Corresponding author; email: fatih.selimefendigil@cbu.edu.tr

a range of Strouhal numbers for Reynolds numbers between 10 to 500. They reported that optimum Strouhal number is between 0.5 to 1 for the best thermal performance and minimum pressure drop. Oztop [10] have studied the mixed convection in a channel with a volumetric heat source and different opening ratio at the exit of the channel for different Richardson numbers between 0.001 to 10. In this study, three different opening ratio at the exit has been considered. It is reported that the Richardson number and exit opening have strong effects on the flow field and thermal characteristics and maximum heat transfer is obtained when the outlet port is placed onto top of vertical wall.

Adding partitions in order to control the fluid field and thermal characteristics of the enclosures have also been extensively studied by many researchers [11-14]. Shi and Khodadadi [11] have studied the flow field and heat transfer characteristic for laminar flow in a lid-driven cavity due to a single thin fin. They showed that placing a fin on the right wall can enhance heat transfer on the left wall but reduce heat transfer on the bottom, right and top walls of the enclosure. Varol *et al.* [13] have studied the effect of an adiabatic thin fin for the fluid flow and heat transfer in a porous triangular cavity for Rayleigh number between 100 to 1000. The effect of the aspect ratio of the triangular cavity, the location of the fin and fin length have been studied numerically. They reported that fins can be used as control parameter for temperature and flow field within the cavity.

In the above mentioned studies, either mixed convection without partitions or effect of the adding partitions on the thermal performance of the systems in the free convection case are analyzed. To the best of the authors' knowledge, a numerical study on the mixed convection in a square enclosure with the addition of an adiabatic fin on one of the walls of the cavity has never been reported in the literature. The aim of the present investigation is to highlight some of the features of the thermal characteristics of such systems which may of interest for the designers.

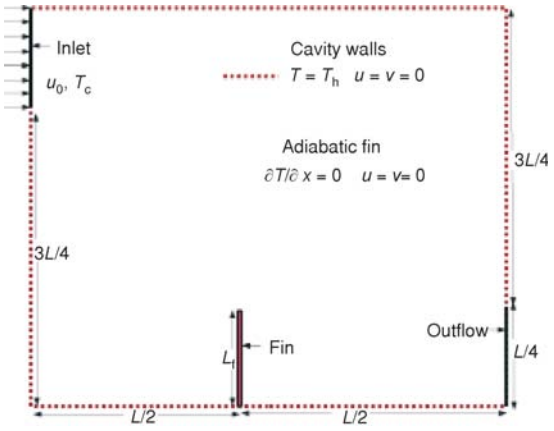

Figure 1. Geometry and the boundary conditions for the cavity with two ventilation ports and an adiabatic thin fin placed in the middle of the wall of the cavity. Air has a uniform velocity u and temperature T_c at the inlet port. All walls of the enclosure are kept at constant temperature T_h

Numerical Simulation

Problem description

A schematic description of the problem is shown in fig. 1. A square enclosure with two ventilation ports is considered. The inlet and outlet ports are placed at the left-top and right-bottom vertical cavity walls. The size of the ports are $L/4$, where L denotes the length of the cavity. All walls of the cavity are kept at temperature T_h. At the inlet port, a uniform velocity is imposed. The width of the square cavity is assumed to be long and the problem can be considered as 2-D.

Working fluid is air with a Prandtl number of Pr = 0.71. The flow is assumed to be 2-D, Newtonian, incompressible and in the laminar flow regime. The physical properties are assumed to be temperature

independent except for the density in the buoyancy force according to Boussinesq approximation.

Governing equations and solution method

By using the dimensionless parameters

$$(U,V)=\frac{u,v}{u_0},\quad (X,Y)=\frac{x,y}{L},\quad P=\frac{p+\rho gy}{\rho u_0^2},\quad \theta=\frac{T-T_c}{T_h-T_c} \tag{1}$$

for a 2-D compressible, laminar, and steady case, the continuity, momentum, and energy equations can be expressed in the non-dimensional form as:

$$\frac{\partial U}{\partial X}+\frac{\partial V}{\partial Y}=0 \tag{2}$$

$$U\frac{\partial U}{\partial X}+V\frac{\partial U}{\partial Y}=\frac{\partial P}{\partial X}+\frac{1}{\mathrm{Re}}\left(\frac{\partial^2 U}{\partial X^2}+\frac{\partial^2 U}{\partial Y^2}\right) \tag{3}$$

$$U\frac{\partial V}{\partial X}+V\frac{\partial V}{\partial Y}=-\frac{\partial P}{\partial Y}+\frac{1}{\mathrm{Re}}\left(\frac{\partial^2 V}{\partial X^2}+\frac{\partial^2 V}{\partial Y^2}\right)+\mathrm{Ri}\theta \tag{4}$$

$$U\frac{\partial \theta}{\partial X}+V\frac{\partial \theta}{\partial Y}=\frac{1}{\mathrm{Pr\,Re}}\left(\frac{\partial^2 \theta}{\partial X^2}+\frac{\partial^2 \theta}{\partial Y^2}\right) \tag{5}$$

The relevant physical non-dimensional numbers are Reynolds number (Re), Grashof number (Gr), and Richardson number (Ri):

$$\mathrm{Re}=\frac{u_0 L}{\nu},\quad \mathrm{Gr}=\frac{g\beta(T_h-T_c)L^3}{\nu^2},\quad \mathrm{Ri}=\frac{\mathrm{Gr}}{\mathrm{Re}^2} \tag{6}$$

Air has a uniform velocity, $U = 1$ and temperature $\theta = 0$ at the inlet port and outflow boundary condition is imposed at the outlet port. All walls of the cavity are kept at high temperature, $\theta = 1$. Thin fin is adiabatic, $\partial\theta/\partial X = 0$. No slip boundary condition ($U = V = 0$) is used for the cavity walls and on the fin. Local Nusselt number is defined as:

$$\mathrm{Nu}_x=\frac{h_x L}{k}=-\left(\frac{\partial\theta}{\partial n}\right)_S \tag{7}$$

where h_x represent the local heat transfer coefficient and k denote the thermal conductivity of air. θ is the non-dimensional temperature which is defined as $\theta = (T - T_c)/(T_h - T_c)$. n and S denote the surface normal component and heated part of the bottom and left vertical side walls of the cavity, respectively. Spatial averaged Nusselt number is obtained after integrating the local Nusselt number along the walls of cavity as:

$$\mathrm{Nu}=\left(\frac{1}{L}\int_0^L \mathrm{Nu}_x\,\mathrm{d}x\right)_{\mathrm{right}}+\left(\frac{1}{L}\int_0^L \mathrm{Nu}_x\,\mathrm{d}x\right)_{\mathrm{left}}+\left(\frac{1}{L}\int_0^L \mathrm{Nu}_y\,\mathrm{d}y\right)_{\mathrm{top}}+\left(\frac{1}{L}\int_0^L \mathrm{Nu}_y\,\mathrm{d}y\right)_{\mathrm{bottom}} \tag{8}$$

Equations (2)-(5) along with the boundary conditions are solved with FLUENT 6.1 solver (a general purpose finite volume solver [15]). The unstructured body-adapted mesh consists of only triangular elements. The choice of which mesh type depends on the application and for moderately complex geometries unstructured grids are generally used. The choice of the

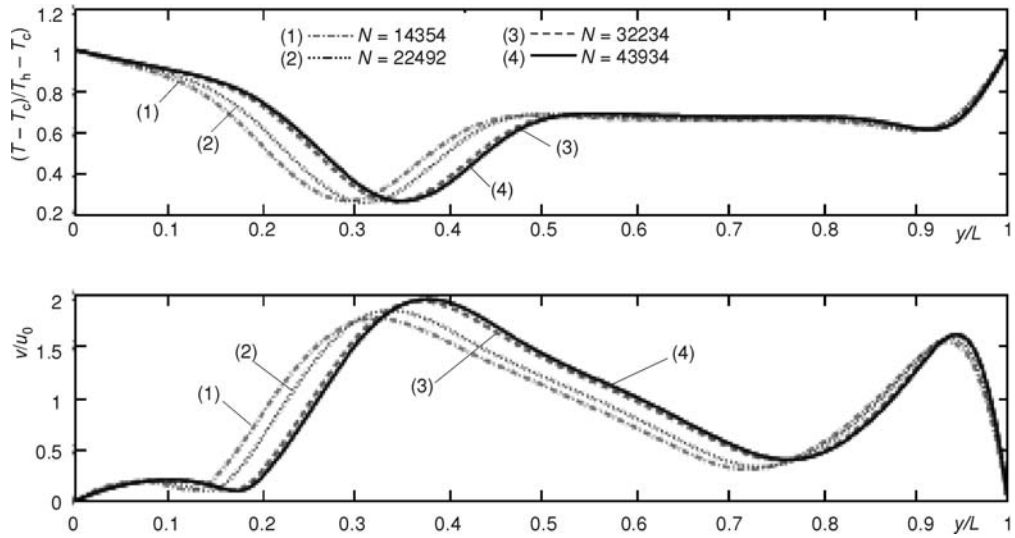

Figure 2. Non-dimensionalized temperature and velocity starting from the middle of the bottom wall ending at the middle of the top wall for different grid sizes at Richardson number of 10

mesh type have effects on the set-up time, computational expense, and numerical diffusion. In the current configuration, a cavity with a fin attached to its of the walls, unstructured mesh is used. For his relatively simple geometry, it does not make a big difference in terms of accuracy and computational time whether we use a structured mesh or an unstructured one. Mesh independence of the solutions has been confirmed for each of the fin heights and for the no-fin case. Non-dimensionalized temperature and velocity magnitude starting from the middle of the bottom wall ending at the middle of the top wall is shown in fig. 2, at different grid sizes for the no-fin case at Richardson number of 10. It is seen that the solution for grid size with 43934 triangular elements is close to the solution with 32234 triangular elements. Grid sensitivity study at Ri = 100, is tabulated in tab. 1. From this table, it is seen that grid size of 32234 is fine enough to resolve the flow and thermal field.

Table 1. Grid size sensitivity study for averaged Nusselt number along the walls at Ri = 100

Grid size	Nusselt number
14364	1.758
22492	1.773
32234	1.782
43934	1.785

A second order accurate spatial discretization, is used. Second order upwind schemes are applied in terms of discretising the momentum and the energy equations. The first-order discretization scheme generally yields better convergence compared to second-order scheme, but will give less accurate results for triangular meshes. In our case, we start with the first-order scheme and then switch to the second-order scheme after some iterations. Pressure implicit with splitting of operators (PISO) algorithm is used for pressure velocity coupling. The steady state PISO algorithm adds an extra correction term for semi-implicit method for pressure linked equations (SIMPLE) algorithm to improve its accuracy per iteration. We also compared the results in terms of computational time and accuracy and negligible differences are seen between SIMPLE and PISO algorithm. The global convergence for the continuity, momentum and energy residuals are set to 10^{-4} , 10^{-5}, and 10^{-5}, respectively. The chosen solver settings are tested for a square

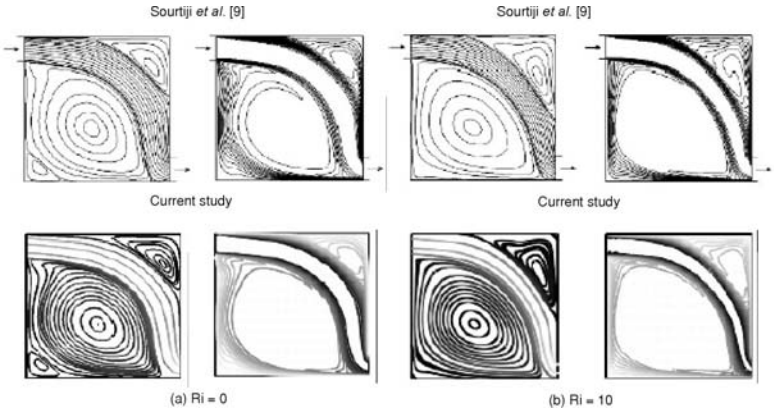

Figure 3. Comparison of the streamlines and isotherms for a cavity with all walls kept at temperature T_h for Richardson number of 0.1 and 1, computed in [9] and computed with the current solver

enclosure without fins with those of [9] for a Reynolds number of 300 (based on the width of the inlet port) for Richardson numbers of 0 and 10 in fig. 3. The streamlines (on the left side) and isotherms (on the right side) computed with two different solvers show similar behavior. The code is further validated against the result of [3]. The comparison is made for the case at Re = 500 (based on the width of the inlet port) and Ri = 0. Figure 4 shows the local Nusselt number distributions along the walls of the cavity for this flow condition computed with the FLUENT code (current settings) and computed in [3]. The comparison results show good overall agreement.

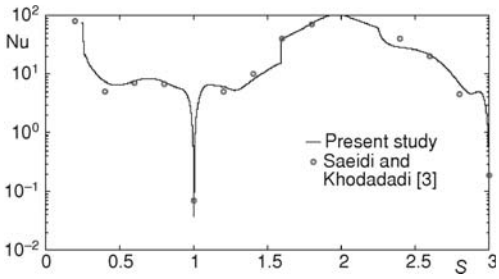

Figure 4. Comparison of local Nusselt number along the three walls of the cavity at Re = 500 and Ri = 0 computed in [3] and computed with FLUENT code

Results and discussion

In the present configuration, the flow field and heat transfer characteristics depend on Reynolds number, Grashof number, Prandtl number, fin length, fin inclination angle, location of the fin on the wall, the width of the inlet-outlet ports, and thermal boundary conditions on the wall. Since a large amount of parameters is necessary to characterize the system, a complete analysis of the system with all parameter combinations are not feasible. In the present study, we fixed some of these parameters and investigate the effects of other varying parameters (fin length, Grashof number, on which wall the fin will be located) on the heat transfer and fluid flow characteristics. In this study, Richardson number is varied between 0.1 and 100 (Ri = 0.1, 1, 10, 100) and Reynolds number based on the length of the square cavity is kept at 300. Prandtl number of the fluid is 0.71.

Streamlines and isotherms

Streamline and isotherm plots when the thin adiabatic fin is attached on the bottom wall for Richardson number of 0.1, 1, 10, and 100 at various fin lengths and no-fin case are shown in fig. 5. In the first row of fig. 5, for the low Ri number, a cell is formed on the left part

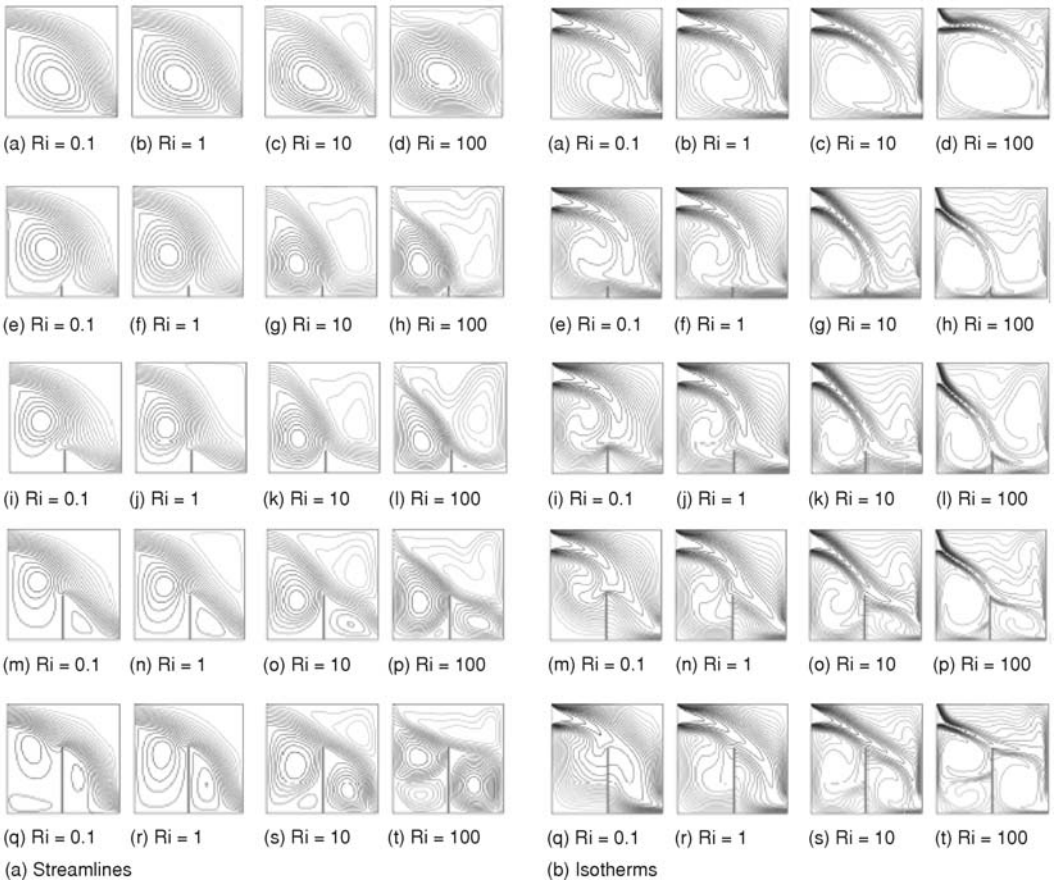

Figure 5. Streamlines and isotherms for no-fin case and different fin lengths ($L_p = 0.1L$, $0.2L$, $0.4L$, $0.6L$) at various Richardson numbers when the fin is positioned on the left wall

of the cavity, occupying half of the cavity. With increasing the Richardson number, buoyancy effects become important, and the cell grows in size and shape. A secondary vortex is also formed on the top-right corner of the cavity for Ri = 10 and 100. For fin length of $L_p = 0.1L$ (second row of fig. 5) , streamlines are more effected for the high Ri numbers (Ri = 10, and 100). At Ri = 100, the cell at the top right corner occupies more of the cavity and the cell at the left part of the cavity decreases in size and shrinks towards left. For fin length of $L_p = 0.4L$ (fourth row of fig. 5), a re-circulation pattern is formed behind the fin near the outlet and grows in size and strength with the increase in Richardson number. For fin length of $L_p = 0.6L$ (fifth row of fig. 5), for the convection dominated mode, the re-circulation patterns in front of and behind the adiabatic thin fin is weak and and grows in size and strength with the increase in Richardson number and at Ri = 100, the cell in front the fin breaks down into two vortices.

A close inspection on the isotherms for different fin lengths in fig. 5 reveal that maximum temperature gradients appear on the bottom and left walls near the inlet and outlet ports for the no-fin case (first row of fig. 5). For fin length of $L_p = 0.1L$ (second row of fig. 5), at high Ri

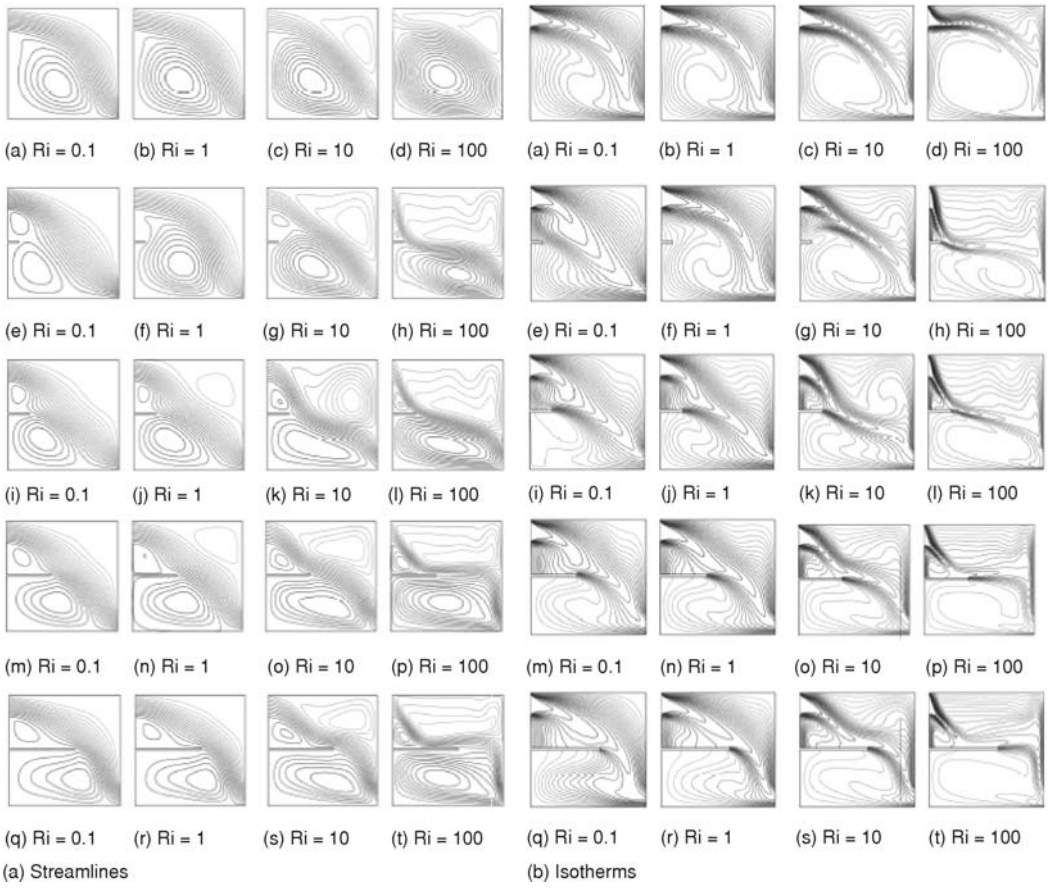

Figure 6. Streamlines and isotherms for no-fin case and different fin lengths ($L_p = 0.1L$, $0.2L$, $0.4L$, $0.6L$) at various Richardson numbers when the fin is positioned on the top wall

numbers (Ri = 10 and 100), the isotherms on the top part of the cavity wall become less clustered and parallel and this shows that heat transfer is not effective in that region of the cavity.

For fin length of $L_p = 0.2L$ (third row of fig. 5), the boundary layer on the bottom wall of the cavity, behind the adiabatic fin and for fin length of $L_p = 0.4L$ (fourth row of fig. 5), the boundary layer in front of the fin near the left bottom corner becomes thicker at Ri = 0.1. For fin length of $L_p = 0.6L$ (sixth row of fig. 5), isotherms spread more into the cavity in front of the fin at Ri = 100.

Streamline and isotherm plots when the thin adiabatic fin is attached on the left wall for Richardson number of 0.1, 1, 10, and 100 at various fin lengths and no-fin case are shown in fig. 6. For fin length of $L_p = 0.1L$ (second row of fig. 6), at Ri = 0.1, a cell is formed at the bottom of the fin, and grows in size for Ri = 1.

At Ri = 10, a vortex is formed right-top and those cells (on the bottom of the fin and on the right-top) become more distorted for Ri = 100. For other fin lengths, similar trends are seen for the streamlines as in the case for $L_p = 0.1L$ and in addition to that, the vortex on the top of the adiabatic fin grows in size and strength for Ri = 10 and 100.

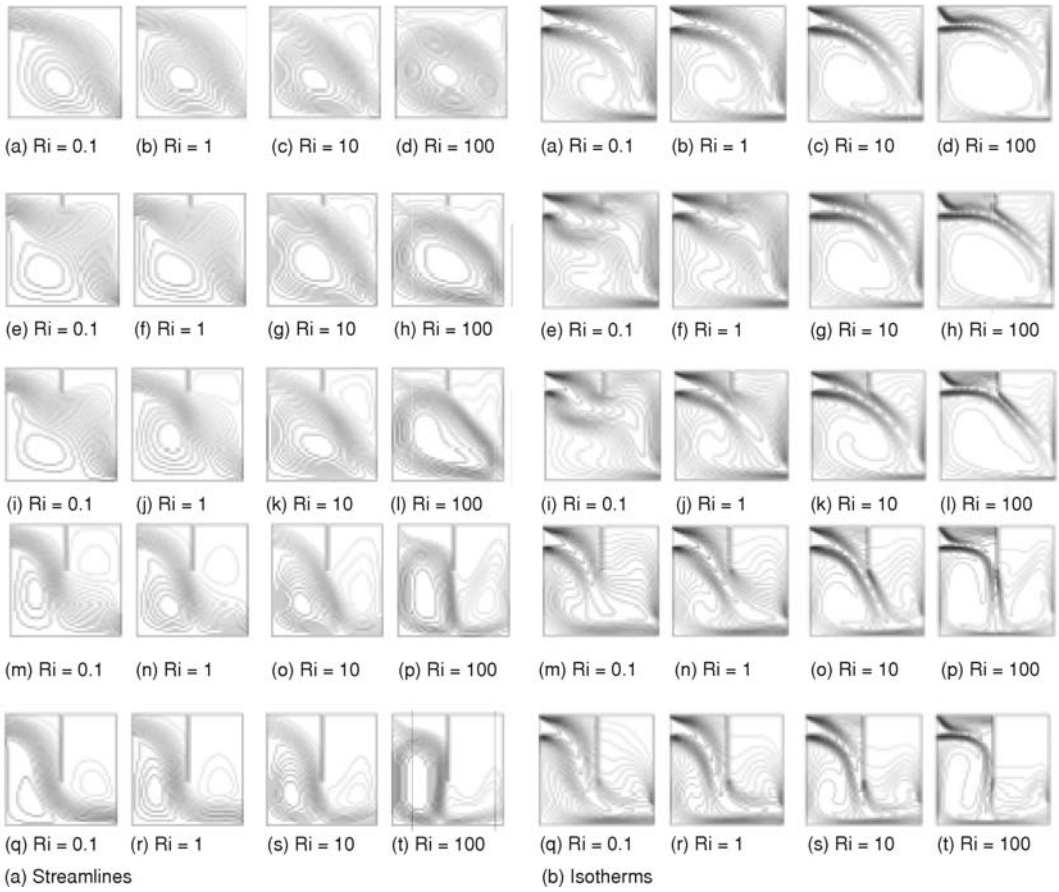

Figure 7. Streamlines and isotherms for no-fin case and different fin lengths ($L_p = 0.1L$, $0.2L$, $0.4L$, $0.6L$) at various Richardson numbers when the fin is positioned on the top wall

Temperature contours in fig. 6 show that for $L_p = 0.1L$, as compared to no-fin case (first row of fig. 6), the isotherms remain almost the same for Ri = 0.1, 1, and 100, but changes significantly for Ri = 100. The closely packed streamlines are directed downwards and on the top isotherms become nearly uniform.

Streamline and isotherm plots when the thin adiabatic fin is attached on the top wall for Richardson number of 0.1, 1, 10, and 100 at various fin lengths and no-fin case are shown in fig. 7. For fin length of $L_p = 0.1L$ (second row of fig. 7), the streamlines show similar trends for different Richardson numbers as in no-fin case. For $L_p = 0.4L$ (fourth row of fig. 7), a cell is formed behind the fin at Ri = 1 and the core of the cell moves towards the outlet. For $L_p = 0.6L$ (fifth row of fig. 7), the top of the cavity on the right of the fin remains stagnant since in this case, fin blocks the airflow towards the top of the cavity. Isotherm plots in fig. 7 show that for $L_p = 0.1L$ (second row of fig. 7), for Ri = 100 when the buoyancy becomes important, the isotherms on the right of the fin becomes less clustered and this means heat transfer in this part is less effective. For $L_p = 0.2L$ and $L_p = 0.4L$, the loosely packed streamlines on the right of the fin is seen at Ri =

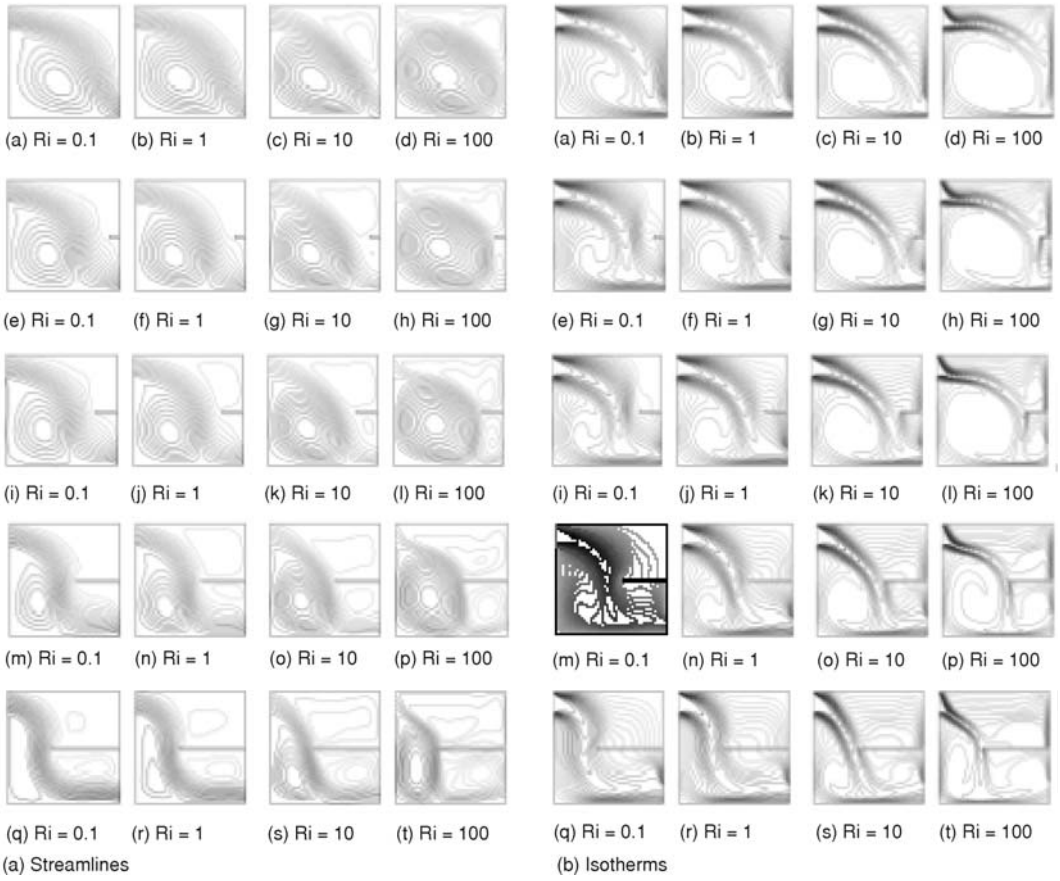

Figure 8. Streamlines and isotherms for no-fin case and different fin lengths ($L_p = 0.1L$, $0.2L$, $0.4L$, $0.6L$) at various Richardson numbers when the fin is positioned on the right wall

= 1 and Ri = 0.1, respectively. For $L_p = 0.6L$, for the case where buoyancy effect are important (Ri = 10 and Ri = 100), the top of the cavity behind the fin remains stagnant and heat transfer in that part less effective.

Streamline and isotherm plots when the thin adiabatic fin is attached on the right wall for Richardson number of 0.1, 1, 10, and 100 at various fin lengths and no-fin case are shown in fig. 8. For fin length of $L_p = 0.1L$ (second row of fig. 8), a vortex is formed on the bottom of the fin for Ri = 100. For $L_p = 0.2L$, this vortex is seen for Ri = 10 and grows in size and strength for Ri = 100. For $L_p = 0.4L$, the cell formed on that location occupies more of the cavity close to the outlet and the cell on the left part of the cavity decreases in size and shrinks towards the left.

Isotherm plots are shown in fig. 8. For $L_p = 0.1L$, at Ri = 0.1, for the convection dominated case, the isotherms on the right-top becomes less dense compared to non-fin case. For Ri = = 100, when the natural convection effects become important, isotherms near the outlet vent, spread more into the cavity. For Ri = 100, with the increase in the fin length, the isotherms on the top of the cavity wall become more flattened and spread more towards the cavity.

Nusselt numbers and pressure drop

Calculated spatial averaged Nusselt number *vs.* Richardson number plots (semi-logarithmic) are shown in fig. 9 for the case when the adiabatic thin fin is placed at the bottom and left wall of the cavity. For the bottom case, heat transfer rate increases with an increase in the Richardson number. At Ri = 0.1, Nusselt number is low compared to no-fin case for all fin lengths and the best performance is obtained for fin length of $L_p = 0.6L$. Minimum Nusselt number is obtained for $L_p = 0.2L$ for the considered Richardson number range. For Ri = 10 and 100, heat transfer enhancement is seen compared to no-fin case for $L_p = 0.6L$. For the left case, in the convection dominated mode at Ri = 0.1, for $L_p = 0.2L$, heat transfer rate is minimum. In the left case, there is no enhancement in the heat transfer for the considered range of Richardson numbers and the best thermal performance is obtained compared to no-fin case when $L_p = 0.6L$. Another observation is that the effect of the fin length on the Nusselt number variation decreases with an increase in the Richardson number.

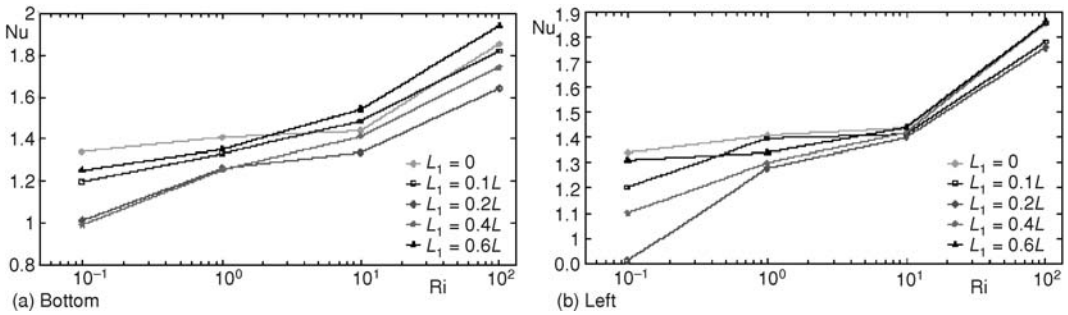

Figure 9. Spatial averaged Nusselt number *vs.* Richardson number for different fin lengths when the position of the fin is at the middle of the bottom wall (top) and left wall (bottom) of the cavity

The pressure drop is defined as the averaged pressure differences between the inlet and outlet ports non-dimensionalized with the square of the velocity at the inlet by the following equation as similar to defined in [3]:

$$C_p = \frac{\overline{p}_{\text{in}} - \overline{p}_{\text{out}}}{0.5u_0^2} \tag{9}$$

where $\overline{p}_{\text{in}}$ and $\overline{p}_{\text{out}}$ denote the length averaged pressure at the inlet and outlet ports, respectively.

Dimensionless pressure drop versus Richardson number for no-fin case and for fin lengths of $L_f = 0.1L$, $L_f = 0.2L$, $L_f = 0.4L$, and $L_f = 0.6L$ are shown in fig. 10. The pressure drop increases in the increasing direction of the Richardson number. When the fin is attached on the bottom wall of the cavity, the length does not have any influence on the pressure drop. When the fin is attached on the left of the cavity, the effect of the fin length on the pressure drop is seen at low Richardson numbers.

Calculated spatial averaged Nusselt number *vs.* Richardson number plots are shown in fig. 11 for the case when the adiabatic thin fin is placed at the top and right wall of the cavity. For the top case, at Ri = 0.1, Nusselt numbers at different fin lengths are less compared to no-fin case. At Ri = 10, heat transfer enhancement is obtained for $L_p = 0.4L$ and $L_p = 0.6L$ and slightly for $L_p = 0.1L$. Adding an adiabatic fin in that case is advantageous for the thermal performance of the system. At Ri = 100, when the natural convection effect become important, heat transfer

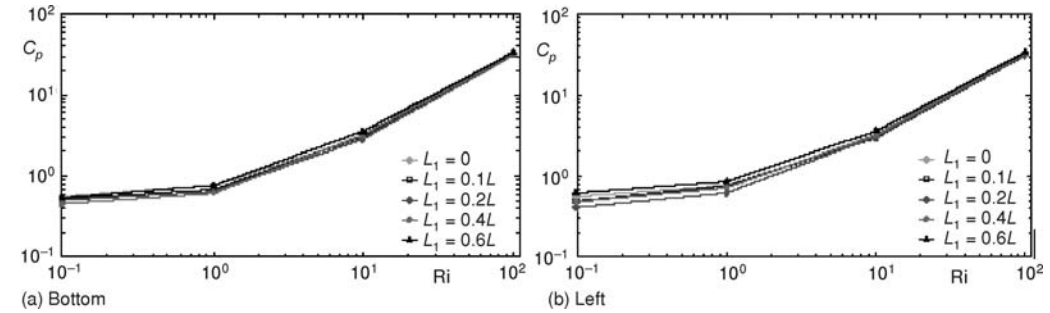

Figure 10. Dimensionless pressure drop *vs*. Richardson number for no-fin case and for different fin lengths when the position of the fin is at the middle of the bottom wall (top) and left wall (bottom) of the cavity

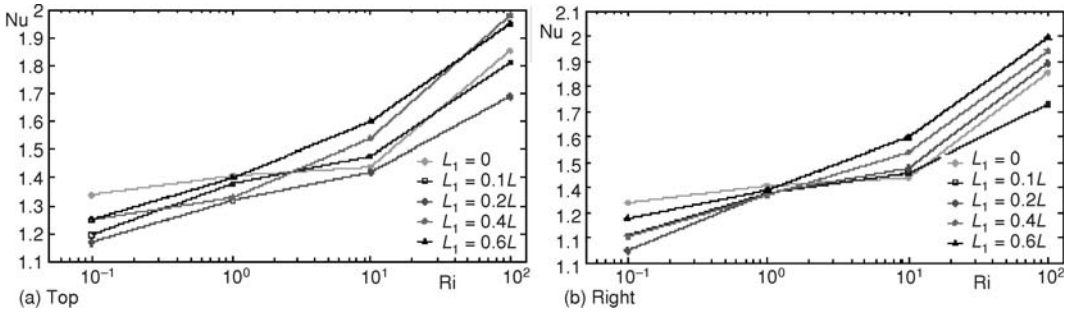

Figure 11. Spatial averaged Nusselt number *vs.* Richardson number for different fin lengths when the position of the fin is at the middle of the top wall (top) and right wall (bottom) of the cavity

enhancement compared to no-fin case is seen only for $L_p = 0.4L$ and $L_p = 0.6L$, and thermal performance degrades for $L_p = 0.2L$. For the bottom case, at Ri = 10 and Ri = 100, heat transfer enhancement is obtained for $L_p = 0.4L$ and $L_p = 0.6L$. At Ri = 100, Nusselt number decreases compared to no-fin case for $L_p = 0.1L$.

Dimensionless pressure drop versus Richardson number for no-fin case and for different fin lengths are shown in fig. 12. When the fin is attached on the top and on the right of the cavity, increasing the fin length will increase the pressure drop at low Richardson numbers.

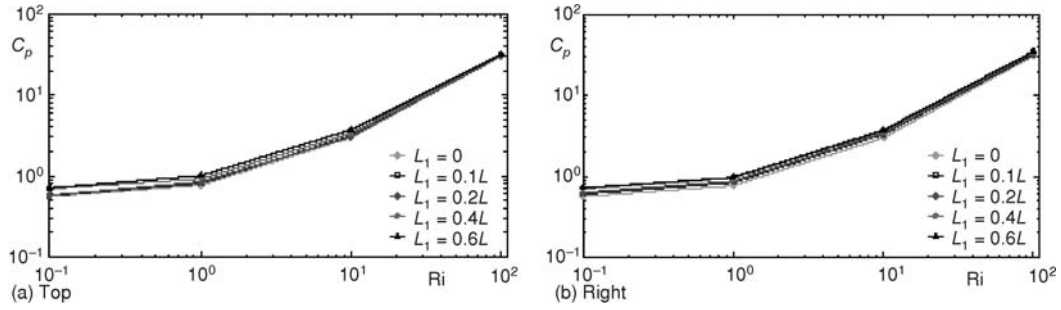

Figure 12. Dimensionless pressure drop *vs.* Richardson number for no-fin case and for different fin lengths when the position of the fin is at the middle of the top wall (top) and right wall (bottom) of the cavity

Conclusions

In this study, the effect of an adiabatic thin fin on the thermal performance of a square cavity with two ventilation ports is numerically analyzed for the mixed convection case for a range of Richardson numbers at Reynolds number of 300. The effect of the fin height, placement of the fin on each of the four walls of the cavity and Richardson number on the heat transfer and fluid flow are numerically analyzed. Following results are obtained.

- Thermal performance of the system increases (heat transfer enhancement is obtained) for fin length of $L_p = 0.6$ at Ri = 10 and 100, when the buoyancy effects become important.
- Adding a fin irrespective of the fin length and position, decreases the thermal performance of the system for the convection dominated case.
- When the adiabatic fin is placed on the bottom, left and top wall of the cavity, the poorest thermal performance is obtained for fin length of $L_p = 0.2$, but for $L_p = 0.1$ when the fin is placed on the right wall of the cavity at Ri = 100.
- Position and length of the fin significantly alters the streamlines and isotherms and hence the thermal performance of the system for the mixed convection case.
- When the fin is attached on the bottom wall of the cavity, the length does not have any influence on the pressure drop.
- When the fin is attached on the top and on the right of the cavity, increasing the fin length will increase the pressure drop at low Richardson numbers.

Length of the fin and the type of the wall where the fin is located have considerable effect on the thermal performance of the system, therefore they can be used as passive control elements for the mixed convection heat transfer. By the proper selection of the fin length, wall location and Richardson number combination, heat transfer augmentation or reduction can be obtained.

The location of the maximum heat transfer can also be controlled with the proper choice of these parameter sets. In the present study, fin inclination angle, effect of Reynolds number, transient effects and width and position of the ports are not considered into account. These parameters may also have influence of the thermal performance of the system.

Nomenclature

C – dimensionless pressure drop $[= (p_{in} - p_{out})/0.5u_0^2]$, [–]
Gr – Grashof number $(= g\beta\Delta TL^3\nu^{-2})$, [–]
g – gravitational acceleration, [ms^{-2}]
h – local heat transfer coefficient, [Wm^{-2}K^{-1}]
k – thermal conductivity of the fluid, [Wm^{-1}K^{-1}]
L – length of the enclosure, [m]
n – unit normal vector on the surface
Nu_x – local Nusselt number, $(= hx/k)$, [–]
Pr – Prandtl number, $(= \nu/\alpha)$, [–]
p – pressure, [Pa]
Re – Reynolds number,$(= u_0L/\nu)$, [–]
Ri – Richardson number number, $(= Gr/Re^2)$, [–]
T – temperature, [K]
u, v – x-y velocity components, [ms^{-1}]
x, y – Cartesian co-ordinates, [m]

Greek symbols

α – thermal diffusivity, [m^{2}s^{-1}]
β – fluid thermal expansion coefficient, [1/K]
θ – dimensionless temperature, $[= (T - T_c)/(T_h - T_c)]$, [–]
ν – kinematic viscosity, [m^{2}s^{-1}]
π – pressure, [Pa]
ρ – density of the fluid, [kgm^{-3}]

Subscripts

c – cold wall
h – hot wall
p – fin

References

[1] Aminossadati, S. M., Ghasemi, A., A Numerical Study of Mixed Convection in a Horizontal Channel with a Discrete Heat Source in an Open Cavity, *European Journal of Mechanics, 28* (2009), 4, pp. 590-598
[2] Boutina, L., Bessaih, R., Numerical Simulation of Mixed Convection Air-Cooling of Electronic Components Mounted in an Inclined Channel, *Applied Thermal Engineering, 31* (2011), 11-12, pp. 2052-2062
[3] Saeidi, S., Khodadadi, J., Transient Flow and Heat Transfer Leading to Periodic State in a Cavity with Inlet and Outlet Ports Due to Incoming Flow Oscillation, *International Journal of Heat and Mass Transfer, 50* (2007), 3-4, pp. 530-538
[4] Selimefendigil, F., Oztop, H., Fuzzy-Based Estimation of Mixed Convection Heat Transfer in a Square Cavity in the Presence of an Adiabatic Inclined Fin, *International Communications in Heat and Mass Transfer, 39* (2012), 10, pp. 1639-1646
[5] Mahmoud, H., *et al*., Numerical Analysis of Recirculation Bubble Sizes of Turbulent Co-Flowing Jet, *Engineering Applications of Computational Fluid Mechanics, 6* (2012), 1, pp. 58-73
[6] Chau, K. W., Jiang, Y. W., A Three-Dimensional Pollutant Transport Model in Orthogonal Curvilinear and Sigma Coordinate System for Pearl River Estuary, *International Journal of Environment and Pollution, 21* (2004), 2, pp. 188-198
[7] Margot, X., *et al*., Numerical Modelling of Cavitation: Validation and Parametric Studies, *Engineering Applications of Computational Fluid Mechanics, 6* (2001), 1, pp. 15-24
[8] Chau, K.W., Jiang, Y. W., 3D Numerical Model for Pearl River Estuary, *Journal of Hydraulic Engineering, 127* (2001), 1, pp. 72-82
[9] Sourtiji, E., *et al*., Heat Transfer Enhancement of Mixed Convection in a Square Cavity with Inlet and Outlet Ports Due to Oscillation of Incoming Flow, *International Communications in Heat and Mass Transfer, 38* (2011), 6, pp. 806-814
[10] Oztop, H. F., Influence of Exit Opening Location on Mixed Convection in a Channel with Volumetric Heat Sources, *International Communications in Heat and Mass Transfer, 37* (2010), 4, pp. 410-415
[11] Shi, X., Khodadadi, J., Laminar Fluid Flow and Heat Transfer in a Lid-Driven Cavity Due to a thin Fin, *J. Heat Transfer, 124* (2002), 6, pp. 1056-1063
[12] Lakhal, E. K., *et al*., Natural Convection in Inclined Rectangular Enclosures with Perfectly Conducting Fins Attached on the Heated Wall, *Heat and Mass Transfer, 32* (1997), 5, pp. 365-373
[13] Varol, Y., *et al*., Effects of thin Fin on Natural Convection in Porous Triangular Enclosures, *International Journal of Thermal Sciences, 46* (2007), 10, pp. 1033-1045
[14] Shaw, H. J., *et al*., Cubic Spline Numerical Solution for Two Dimensional Natural Convection in a Partially Divided Enclosure, *Numerical Heat Transfer, 12* (1987), 4, pp. 439-455
[15] ***, Fluent Inc., FLUENT User's Guide, Lebanon, N. H., USA, 2005

Paper submitted: June 8, 2012
Paper revised: April 4, 2013
Paper accepted: April 24, 2013